Unified R-Matrix-Plus-Potential Analysis for $^{16}O + n$ Cross Sections

C. H. Johnson
Oak Ridge National Laboratory, Oak Ridge, Tennessee 37830*
(Received 15 August 1972)

A multilevel two-channel R-matrix analysis is made for both the neutron total and angle-integrated (n,α) cross sections of ^{16}O for 0–5.8-MeV neutrons. Off-resonant phase shifts are described by scattering in a real Woods-Saxon local potential with a spin-orbit term and a parity dependence for the well depths. The well parameters are chosen to bind the $1d_{5/2}$ and $2s_{1/2}$ levels at the energies of the lowest two states in ^{17}O and the quasibound $1d_{3/2}$ level at the centroid of five observed $\frac{3}{2}^+$ resonances. The $1d_{3/2}$ level is replaced by these five fragments which contain nearly 100% of the $1d_{3/2}$ strength and have their eigenenergy centroid at 5.74 MeV in ^{17}O. The 5.08-MeV level in ^{17}O has 69% of the strength. The R-matrix boundary radius must be chosen carefully inside the tail of the potential in order to subtract the $1d_{3/2}$ state and in order to place the unbound $2p$ and $1f$ states at energies consistent with the observed p- and f-wave fragments. Spectroscopic factors are deduced for 26 levels in ^{17}O between 4.5 and 9.5 MeV and the sums of these factors are 1% for $J^\pi = \frac{1}{2}^+$; 5% for $\frac{1}{2}^-$; 12% for $\frac{3}{2}^-$; 99% for $\frac{3}{2}^+$; 0.1% for $\frac{5}{2}^+$; 1% for $\frac{5}{2}^-$; and 14% for $\frac{7}{2}^-$. Thus, the observed single-particle structure of ^{17}O in both the bound and unbound region is described by an R-matrix-plus-potential analysis.

I. INTRODUCTION

Frequent objections are lodged against the R-matrix theory[1,2] because of the arbitrary nature of the boundary radius and the related arbitrariness of the reduced widths and the R^∞ functions for distant resonances. In this paper most of this arbitrariness is removed by the use of a carefully chosen diffuse-edge potential to describe the off-resonant scattering. The boundary radius is restricted to a limited region inside the tail of the potential and the reduced widths are deduced relative to the single-particle R-matrix states for this potential.

The paper is devoted to the neutron total and angle-integrated (n, α) cross sections for ^{16}O in a broad neutron energy region from thermal to 5.8 MeV. There is only one neutron channel for each J^π and the resulting multilevel two-channel R matrix can be inverted.[2] In the past the full power of the theory for total cross sections has generally not been utilized. Within the region studied here, except near the upper end, fluctuations in the total cross sections must arise from the local resonances and, since these cross sections have been measured with such good resolution and good statistics over broad energy regions, a detailed multilevel analysis can extract information not available from other measurements. The data included here on total cross sections are from a companion paper[3] and from several papers[4-7] from Wisconsin. The $^{16}O(n, \alpha)^{13}C$ cross sections are from data on the inverse reaction by Bair and Haas.[8] The resulting fit to these data is good and the level parameters are discussed here and in the companion paper.[3]

The off-resonant scattering is also significant. For example, theoretical calculations[9-11] based on two-body forces have been compared previously to the off-resonant scattering of neutrons from ^{16}O. In an R-matrix analysis, the off-resonant cross sections are attributed to hard-sphere scattering plus the tails from all distant resonances. Traditionally distant levels are introduced as R^∞ functions with adjustable energy coefficients; however, the off-resonant scattering can be attributed[12,13] to the real part of the optical-model potential. In fact, this provides significant data on the potential. The phase shift for a potential can be expanded into a sum of hard sphere and plus "resonant" phases, the latter being attributed to an R function. In this paper, I equate this R function to R^∞. Special treatment is required for $d_{3/2}$ waves because the $1d_{3/2}$ resonance is inside the region of interest; I subtract the $1d_{3/2}$ term and equate the remaining R function to R^∞. The final fit to the off-resonant scattering involves seven parameters with six for the potentials and one for the R-matrix boundary; however, only four of these are adjusted to fit the scattering. The other three are used to give the energies of the bound $2s_{1/2}$ and $1d_{5/2}$ states and the quasibound $1d_{3/2}$ state.

The potential plays a second role in the assignment of spectroscopic factors. For years it has been realized[12-15] that the traditional Wigner-Teichman[16] single-particle estimate should be replaced by one deduced from an appropriate potential. This is fairly straightforward if the observed

resonances can be compared directly with that for a quasibound single-particle state. Even then the spectroscopic factors are somewhat ambiguous because the width of a resonance for a potential depends on the well parameters, especially on the surface diffuseness. In this paper, I choose the potential to fit not only the energies of the three s-d states but also the s-wave phase shifts below 3 MeV. In essence, the latter requirement restricts the width of the bound s state. This leads to a certain width for the $1d_{3/2}$ resonance and, in the final analysis, to a spectroscopic sum of almost unity for the five $\frac{3}{2}^+$ states observed below 9.5 MeV in ^{17}O.

This takes care of the $1d_{3/2}$ state but leaves the single-particle widths of the higher $2p$ and $1f$ states uncertain. Heavier nuclei have bound $2p$ and $1f$ states but, as the nuclei become lighter approaching ^{17}O, those states rise up and disappear into the continuum. Thus, the potentials used here do not have well-defined p- and f-wave resonances, except possibly $1f_{7/2}$. (If each phase-shift curve were plotted with zero phase at zero energy, it would finally decrease to $-n\pi$ at infinite energy, where n is the number of bound states of the potential.[17]) One approach to this problem is to increase the well depth temporarily to bring the $2p$ and $1f$ states back down below the barrier where their widths can be calculated. That is a questionable procedure. But the imposition of R-matrix boundary conditions creates $2p$, $1f$, and higher states that can be taken seriously[17] for shell-structure calculations. The eigenenergies depend on the arbitrary boundary radius and, off hand, it might seem that the reduced widths have little physical significance. The work of Vogt *et al.*[12] suggests, however, that the reduced widths are meaningful providing the boundary radius is near the center of the diffuse surface. Then the reduced width of a single-particle state is not very sensitive to whether the state is quasibound or not and the spectroscopic factors for observed levels can be deduced by comparison.

The discussion is in terms of real phase shifts. The total cross section for lJ neutrons of center-of-mass energy E, or momentum $\hbar k$, is

$$\sigma_T^{lJ} = (J+\tfrac{1}{2})\frac{2\pi}{k^2}(1-\mathrm{Re}U_{lJ}) \tag{1}$$

and, assuming neutron capture is negligible, the (n,α) cross section is

$$\sigma_{n,\alpha}^{lJ} = (J+\tfrac{1}{2})\frac{\pi}{k^2}(1-|U_{lJ}|^2), \tag{2}$$

where U_{lJ} is the scattering matrix element. In terms of a real phase shift,

$$U_{lJ} = |U_{lJ}|e^{2i\delta_{lJ}}. \tag{3}$$

We first treat the single-channel case for which the $|U_{lJ}|$ is unity and the R matrix is an R function. The modifications in Sec. V for the α channel are relatively minor.

II. POTENTIALS AND THEIR R FUNCTIONS

The potential is a Woods-Saxon well with a Thomas-type spin-orbit term:

$$V(r) = V_0\rho(r) - V_{so}\frac{\vec{l}\cdot\vec{\sigma}}{r}\frac{d\rho(r)}{dr}, \tag{4}$$

where

$$\rho(r) = (1+e^{(r-R)/a})^{-1},$$

$$R = r_0A^{1/3},$$

and $A=16$ for ^{16}O. For simplicity the parameters are introduced as if they were chosen prior to the R-matrix analysis. Actually, a preliminary analysis was required to determine the off-resonant effects of local resonances. The observed off-resonant scattering requires different parameters for s- and d-waves than for p waves.

Figure 1 illustrates the manner in which I chose

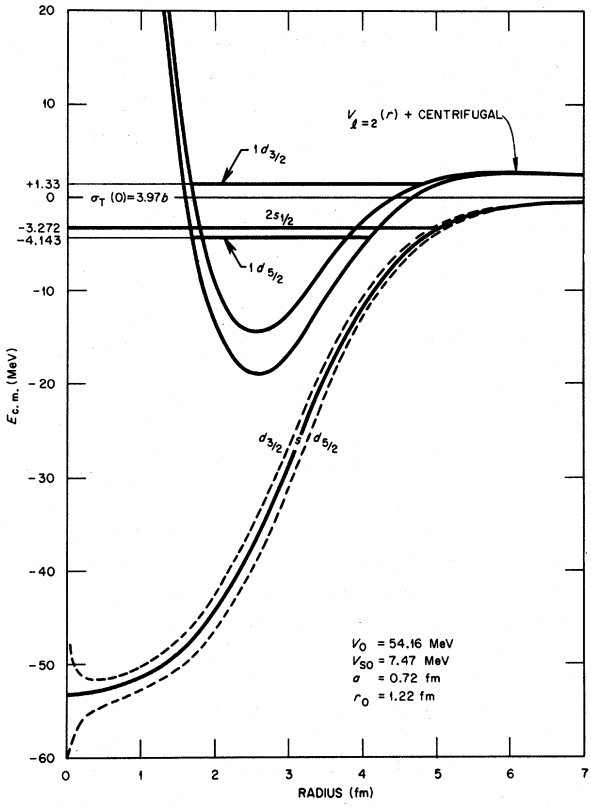

FIG 1. The potentials. The listed even-parity parameters are chosen to fit the experimental energies of the s and d states and the thermal s-wave scattering as shown in the upper part of the figure. The odd-parity potential (not plotted) has the same r_0 and a with $V_0=46$ MeV and $V_{so}=3$ MeV.

the four parameters for the even-parity potential to fit four observed properties of the single-particle s-d states in ^{17}O. (These calculations require different subroutines for the bound[18] and unbound[19] region.) The $2s_{1/2}$ and $1d_{5/2}$ states are bound at the observed energies[20] of the single-particle[21] states, the quasibound $1d_{3/2}$ state is near the eigenenergy centroid for five $\frac{3}{2}^+$ resonant states, and the scattering phase shifts arising from the bound s state agree with the nonresonant s-wave phase shifts for neutrons below 3 MeV. More specifically for s waves, the potential is such that the thermal cross section obtained by combining the resonant tails of the R matrix with the potential phase shift agrees with the known thermal value[22] of 3.74 ± 0.06 b. Figures 2 and 3 include the s- and d-wave phase shifts for scattering in this potential. The dashed curve in Fig. 2 shows the $1d_{3/2}$ resonance which has a width determined by the barrier of the combined nuclear and centrifugal potentials. For the analysis (Sec. IV) this state is subtracted out as indicated by the curve labeled "$d_{3/2} - 1d_{3/2}$."

The p- and f-wave phase shifts for the even-parity potential (dashed curves in Fig. 3) are not consistent with the off-resonant cross sections. The potential $p_{3/2}$ phase shifts are too large to fit some data, such as the 2.35-MeV minimum; and the curve for $p_{1/2}$ is positive, whereas scattering measurement,[23-25] as well as the present results, show that it should be negative below 3 MeV. Also the shape[3] of the $\frac{7}{2}^-$ resonance at 3.766 MeV shows that the $f_{7/2}$ phase shifts are too large at the higher energies. Some of the parameters must be changed. Since the energies of the single-particle states are affected mostly by the well depths, and the reduced widths by the surface parameters, we can facilitate comparisons of observed and single-particle reduced widths by changing only the well depths to give the odd-parity potential. To fit p waves I choose $V_0 = 46$ MeV and $V_{so} = 3$ MeV; I then use the same potential for f waves. The phase shifts are plotted as solid lines in Fig. 3. (The final fit might be improved by a potential with more negative $p_{1/2}$ phase shifts.)

The potential phase shifts can be expanded into hard sphere and "resonant" components familiar to the R-matrix theory[1, 2, 12]:

$$\delta_{lJ} = \varphi_{lJ} + \delta^R_{lJ}, \tag{5}$$

where

$$\tan\varphi_{lJ} = (F_{lJ}/G_{lJ})_{r=r_b} \tag{6}$$

and

$$\tan\delta^R_{lJ} = \left.\frac{P_{lJ}R^p_{lJ}}{1 - S^0_{lJ}R^p_{lJ}}\right|_{r=r_b} \tag{7}$$

with $S^0_{lJ} = S_{lJ} - b_{lJ}$.

The potential R function is given by

$$R^p_{lJ} = (f_{lJ} - b_{lJ})^{-1},$$

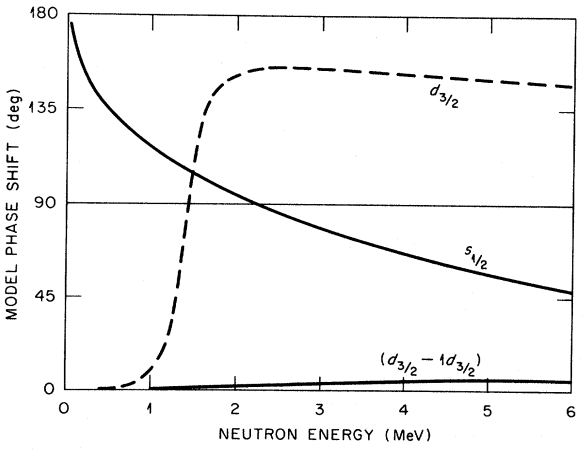

FIG. 2. The $d_{3/2}$ and $s_{1/2}$ phase shifts for the even-parity potential. The $1d_{3/2}$ resonance is subtracted to give the "$d_{3/2}$-$1d_{1/2}$" curve. The solid curves are used for the R-matrix analysis.

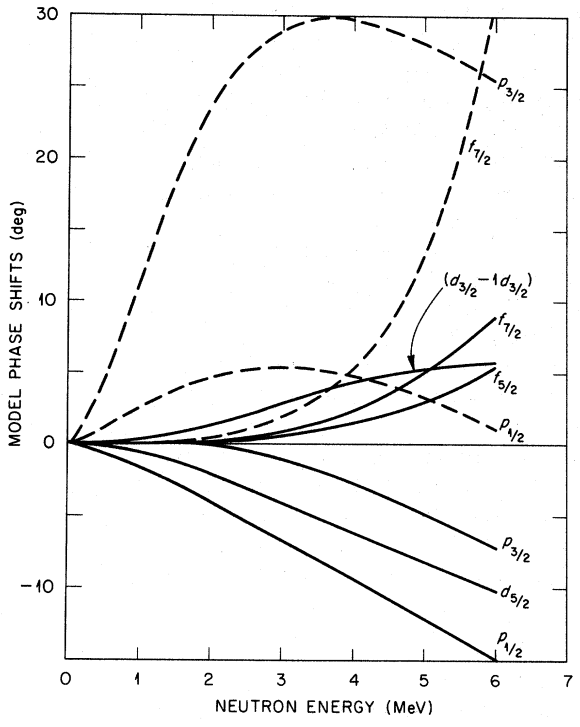

FIG. 3. Potential scattering phase shifts. The d-wave curves and the dashed curves for p and f waves are for the even-parity potential; the solid curves for p and f waves are for the odd-parity well. The $f_{5/2}$ curves are nearly the same for both wells. The solid curves are used for the R-matrix analysis.

where

$$f_{lJ} = \frac{r}{u_{lJ}} \frac{du_{lJ}}{dr}\bigg|_{r=r_b}, \tag{8}$$

and u_{lJ} is the radial part of the wave function that is regular at the origin.

For the moment the radius r_b is arbitrary. If it is outside the well, F_{lJ} and G_{lJ} are the usual wave functions F_l and G_l, and P_{lJ} and S_{lJ} are the corresponding penetrability and shift factors[2] P_l and S_l. If r_b is inside, F_{lJ} and G_{lJ} are the inward continuations[12] of F_l and G_l, and P_{lJ} and S_{lJ} are corresponding modifications of P_l and S_l. Figure 4 shows the modified penetrabilities, calculated in one or the other of the above potentials and divided by the usual penetrabilities for the same radius in the absence of a potential. (The radius, $r_b = 3.86$ fm $= 1.256 r_0 A^{1/3}$, is used below in the final analysis.)

The relative contributions of the hard-sphere and "resonant" components in Eq. (5) depend[17] on the arbitrary radius r_b. As r_b increases, φ_{lJ} becomes more negative and δ^R_{lJ} more positive while δ_{lJ} remains unchanged. Figure 5 shows examples for $p_{3/2}$ waves for the odd-parity potential. The solid curve is the potential phase shift and the broken curves are the resonant and hard-sphere components for two different r_b, one just outside of the well at 7 fm and the other inside at 3.86 fm. Although true resonances do not occur in δ_{lJ}, "resonances" do occur in δ^R_{lJ} where it passes upward through $(n+\frac{1}{2})\pi$. The spacings and widths of these "resonances" increase with decreasing r_b. This dependence of r_b does not occur if the "resonance" corresponds to a true δ_{lJ} resonance such as the one for the quasibound $1d_{3/2}$ state. In that case the hard-sphere component is small and the "resonance" in δ^R_{lJ} is nearly independent of r_b unless r_b is very large.

Up to this point b_{lJ} has been arbitrary. If we now impose the boundary condition, $f_{lJ}(E) = b_{lJ}$ at r_b, we can solve for the eigenenergies and expand the potential R function;

$$R^p_{lJ} = \sum_{p=1}^{\infty} \frac{\gamma_{plJ}{}^2}{E_{plJ} - E}, \tag{9}$$

where the reduced widths are calculated from the surface wave functions at the eigenenergies

$$\gamma_{plJ}{}^2 = \frac{\hbar^2}{2\mu r} u_{plJ}{}^2\bigg|_{r=r_b}. \tag{10}$$

In the following analysis we introduce the "exact" R function R^p_{lJ} into the R matrix and do not find the terms of the expansion, except for $1d_{3/2}$; nevertheless, we must be aware that a unique expansion exists for a given set of boundary conditions. A "natural" value for b_{lJ} is that which makes S^0_{lJ} vanish at one of the energies where $\delta^R_{lJ} = (n+\frac{1}{2})\pi$. Then, for that resonance, the eigenenergy is the resonant energy. The other levels in the expansion correspond on a one-to-one basis to the bound states and to the other resonances.

Although the number of bound and quasibound states are determined by the potential, the spacing and widths of the unbound R-function states depend on the boundary radius. Figure 6 shows the first unbound states for two values of r_b for each partial wave in the appropriate even or odd potential. Natural boundary conditions have been imposed; thus, for example, the $2p_{3/2}$ energies are the same

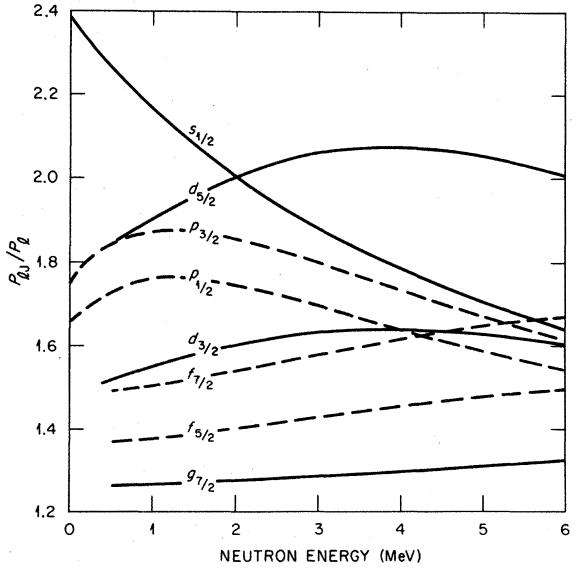

FIG. 4. Ratios of modified to usual penetrabilities at the same radius, 3.86 fm. The solid and dashed curves refer to the even and odd potentials.

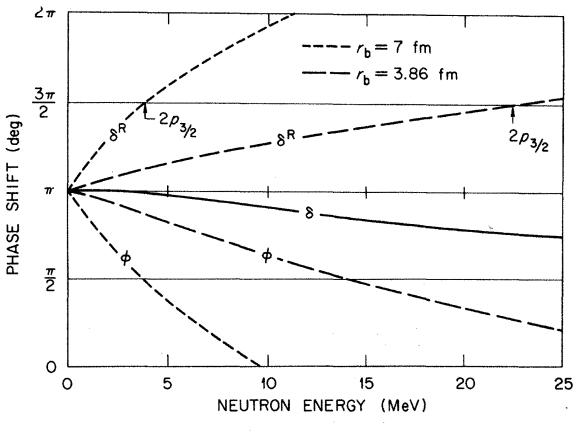

FIG. 5. Resonant and hard-sphere components of the $p_{3/2}$ phase shifts for two different r_b. Arrows indicate the $2p_{3/2}$ "resonance."

as indicated by arrows in Fig. 5. We see that r_b is an additional model parameter. Although it does not affect the total scattering phase shifts for the potential, it does affect the hard-sphere and "resonant" components and it becomes important when the potential is incorporated into the R-matrix theory to describe the actual phase shifts.

III. SINGLE-CHANNEL MULTILEVEL R FUNCTION

For the moment we leave the model and discuss the actual scattering. The potential R function in Eq. (7) must be replaced by one representing the internal wave functions at the surface. The single-channel multilevel R function is

$$R_{lJ}=\sum_{\lambda=1}^{\infty}\frac{\gamma_{\lambda n lJ}{}^2}{E_{\lambda lJ}-E}, \tag{11}$$

where $E_{\lambda lJ}$ and $\gamma_{\lambda n lJ}{}^2$ are eigenenergies and neutron reduced widths for actual levels in ^{17}O. Following the usual procedure we separate this sum into two parts;

$$R_{lJ}=\sum_{\lambda=1}^{N_{lJ}}\frac{\gamma_{\lambda n lJ}{}^2}{E_{\lambda lJ}-E}+R_{lJ}^{\infty}, \tag{12}$$

where the parameters in the summation are to be adjusted to fit the widths and positions of the N_{lJ} levels observed within the region of interest, and the residue R_{lJ}^{∞} of distant levels is to be chosen to fit the off-resonant phase shifts.

Both R_{lJ}^{∞} and the hard-sphere phase shift φ_{lJ} affect the off-resonant scattering. Also both affect the shapes of resonances but in different ways; changes in φ_{lJ} merely alter the pattern of interference between resonant and potential scattering whereas changes in R_{lJ}^{∞} also alter the resonant widths. It would be convenient if we could adjust φ_{lJ} rather than R_{lJ}^{∞} to avoid altering the widths, but this procedure is not allowed; once r_b is chosen, φ_{lJ} becomes a known property of the exterior and the R function is to be adjusted to describe the unknown properties of the interior. In some cases it is important to recognize the effects of R^{∞} on the observed widths.

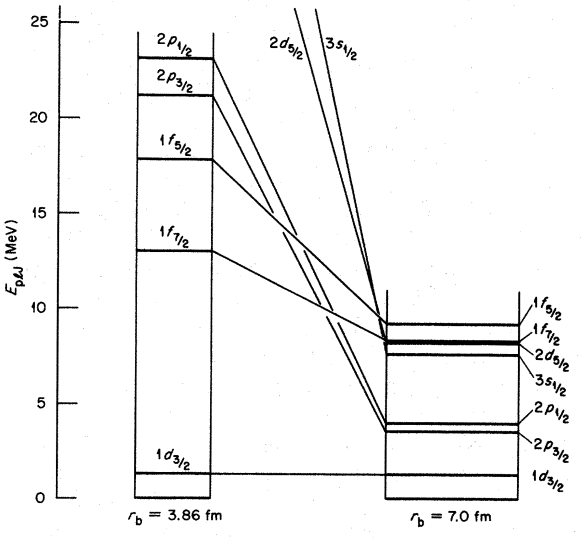

FIG. 6. Energies for the first unbound R-function states for the natural boundary conditions for two boundary radii. The even- and odd-parity levels correspond to the even and odd potentials.

Figure 7 illustrates interference effects for two overlapping $\frac{3}{2}^+$ resonances. No other resonances are included here except those in R^{∞}. For the solid curve the ratio of observed widths is 6/1 even though the ratio of reduced widths is 2/1. If a narrow level occurs within the width Γ_n of a broad one, it always appears narrower than expected from the familiar single-level expression, $\Gamma_n=2P\gamma_n{}^2$. The other two curves show related effects; both resonances become broader for $R_{3/2^+}^{\infty}=+0.5$ and narrower for -0.5. The sign of this effect, i.e., whether a resonance is made broader or narrower by interferference with R^{∞} depends in part on the boundary conditions. Here $S^0=0$ at 1.42 MeV. (The eigenenergies have been adjusted to make the peaks occur at the same energies for all three curves.)

These effects make it difficult to define resonant energies and observed widths. I define a resonant energy by reference to the single-level approximation. Near each level an expansion could be made[2] for Eq. (5) in which only a single level would be included in a new resonant phase shift $\delta_{lJ}^{R'}$, and the tails of all of the other resonances including R_{lJ}^{∞} would be incorporated into a modified φ_{lJ}' term. Then the resonant energy would be where $\delta_{lJ}^{R'}=\pi/2$ or, equivalently, where $\delta_{lJ}^{R'}$ has a point of inflection with maximum slope. If we assume φ_{lJ}' varies linearly with energy, we

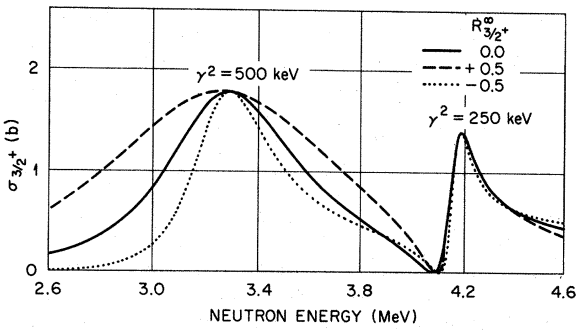

FIG. 7. Interference of adjacent $\frac{3}{2}^+$ resonances with each other and with R^{∞}.

can find the point of inflection of the *total* phase shift. Thus, I define E_{rlJ} as an energy where

$$\frac{\partial^2 \delta_{lJ}}{\partial E^2} = 0 \,. \tag{13}$$

I then define the observed width $\Gamma_{\lambda n lJ}$ as the energy difference between points which are $\pi/4$ on either side of the phase shift at E_{rlJ}. For a narrow level this is the same as obtained in the single-level expansion and for a wide level it is about that obtained by a phenomenological Breit-Wigner fit with a constant potential term. In general the single-level expression, $\Gamma_n = 2P\gamma_n^2$, is a good approximation only for isolated levels.

IV. R^∞ AND THE BOUNDARY CONDITIONS

For all but $d_{3/2}$ waves I replace R_{lJ}^∞ by the R function from one or the other of the above potentials; thus,

$$R_{lJ}^\infty = R_{lJ}^p \,. \tag{14}$$

For $d_{3/2}$ waves, I subtract the $1d_{3/2}$ state;

$$R_{3/2^+}^\infty = R_{3/2^+}^p - \gamma_{1d_-}^2/(E_{1d_-} - E) \,. \tag{15}$$

Some justification for this procedure has been given by Westin and Adams.[13]

The concepts embodied in Eqs. (14) and (15) are shown schematically in Fig. 8, which applies to neutrons on ^{16}O and is based partially on the results of the R-matrix fit. Within our energy region of 0–5.8 MeV there are obviously three possibilities for each partial wave; either the observed fragments add up to a negligible fraction of the single-particle strength, or to nearly all of it, or to a nonnegligible fraction. The estimates from Eq. (14) or (15) are rather good for the all-or-none limits but approximate for the intermediate case. Figure 8(a) represents the case of negligible fragments. The observed $\frac{1}{2}^+$ and $\frac{5}{2}^+$ resonances do have small widths and the bound states contain most of the nearby single-particle strengths. The sum of reduced widths is also small for $f_{5/2}$ neutrons. In these cases Eq. (14) should be a good approximation. Figure 8(b) illustrates the other limit, which applies for $d_{3/2}$ neutrons. The observed fragments add up to nearly 100% of the $1d_{3/2}$ strength and Eq. (15) should be a good estimate for the remaining distant states. Figure 8(d) illustrates for p waves. The observed sum is about 10% for $p_{1/2}$ or $p_{3/2}$; thus, the single-particle state must be relatively far away and Eq. (14) is a fairly good approximation. The sum for $f_{7/2}$ resonances is slightly larger; Eq. (14) is still adequate but it would probably fail rapidly if the analysis were extended to higher energies.

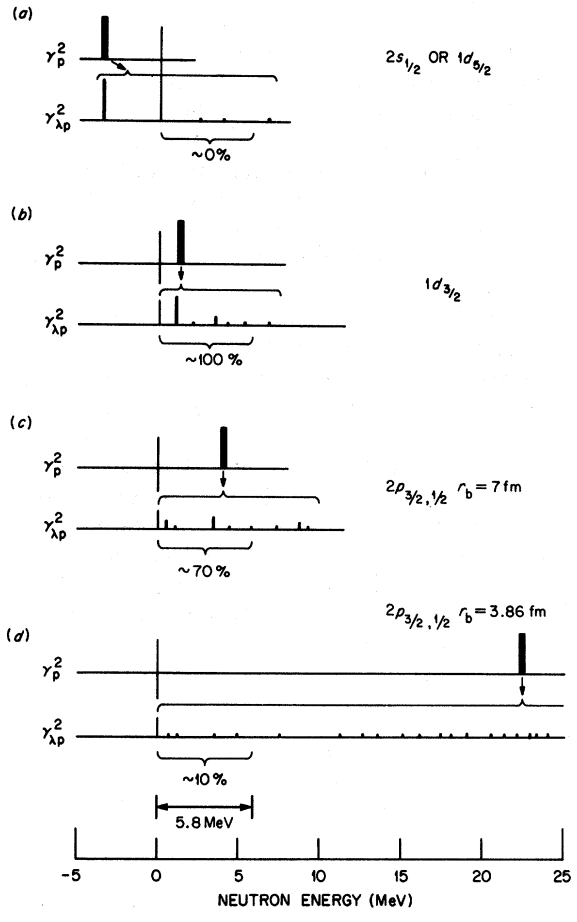

FIG. 8. Fragments of single-particle states: (a) The bound $d_{5/2}$ and $s_{1/2}$ states contain nearly all of the single-particle strength. (b) The $d_{3/2}$ fragments from 0 to 5.8 MeV are nearly 100% of the $1d_{3/2}$ strength. (c) and (d) The p-wave fragments for 0 to 5.8 MeV depend on the assumed radius r_b.

The boundary radius must be chosen carefully. If the only purpose were to subdivide the potential phase shifts into "resonant" and hard-sphere components, the radius would be arbitrary; but for the R-matrix analysis the radius must be near the nuclear surface. This still leaves some freedom of choice and, specifically, it allows boundaries either inside or outside the tail of the potential. Takeuchi and Moldauer[17] used a potential similar to ours for the $n + {}^{16}$O system and placed the boundary outside at either 7 or 10 fm. Westin and Adams[13] insist that the boundary be outside. Vogt *et al.*[12] found good reason to put it inside. I put the boundary inside for theoretical reasons, *a priori*, and for reasons, *a posteriori*, specifically related to $n + {}^{16}$O.

The *a priori* reasons follow Vogt's analysis.[12] He showed that a boundary near the center of the surface allows one to interpret the wave proper-

ties in terms of the penetration of the barrier, the reflection at the surface, and the resonant behavior in the interior. The boundary represents a "sphere of ignorance"; it seems reasonable to make this sphere small by placing r_b inside of the tail of the potential so that the R function represents only the resonant properties of the interior, not the additional effects of penetration.

The work of Vogt *et al.*[12] shows also that an inner boundary should be used to derive spectroscopic factors consistently for all partial waves. If we were concerned here only with the $\frac{3}{2}^+$ states, the radius would not be critical in this regard because, with minor corrections for penetrabilities, the widths of the five $\frac{3}{2}^+$ fragments could be compared directly with the nearby $1d_{3/2}$ resonance. For other partial waves, however, there are no such resonances. To approach this problem let us define a dimensionless single-particle reduced width;

$$\theta_{pIJ}{}^2 = \frac{\gamma_{pIJ}{}^2}{\hbar^2/\mu r_b{}^2}. \tag{16}$$

Figure 9 shows $\theta_{pIJ}{}^2$ for the above potential as a function of r_b for the first unbound states. (If r_b = 3.86 or 7 fm, these widths refer to the levels in Fig. 6.) The barrier effects are relatively large for the quasibound $1d_{3/2}$ state but not for the other R-function states. Thus, the spread in $\theta_{pIJ}{}^2$ is less if the boundary is inside at about 3.5 to 4 fm. Furthermore, the dependences on the well depths and on the principal quantum number for a given partial wave are less at an inner boundary. For simplicity I decided, *a priori*, to let r_b = 3.86 fm so that the dimensionless $1d_{3/2}$ width is exactly unity. Let us define a dimensionless width for an observed resonance,

$$\theta_{\lambda nIJ}{}^2 = \left.\frac{\gamma_{\lambda nIJ}{}^2}{\hbar^2/\mu r_b{}^2}\right|_{r_b = 3.86\ fm}. \tag{17}$$

For a $d_{3/2}$ resonance, this is the spectroscopic factor. For other resonances it may be 30 to 50% too large. [In retrospect, the figure shows that a boundary radius of 3.5 fm with a corresponding change in Eq. (17) would give more realistic spectroscopic factors for all but f waves.]

Now, let us consider the reasons revealed, *a posteriori*, for an inner radius. Since the solid curves in Figs. 2 and 3 give a rather good fit in the final analysis, they are essentially correct whether a potential model is used or not. If we were to choose an outer radius of 7 fm, the off-resonant values for δ_{lJ}^R would have to be large and positive (except for s waves) to compensate for the large negative hard-sphere phase shifts. The energies of the associated single-particle states would be located as shown by the 7-fm diagram in Fig. 6. The proximity of these states to the region of the analysis is inconsistent with the small widths actually observed for all but the $d_{3/2}$ resonances. Even for $d_{3/2}$ the 7-fm boundary would introduce a second single-particle state near 6.5 MeV in contradiction to the observed fragments. This inconsistency is particularly obvious for p waves because the $2p$ states for r_b = 7 fm are actually inside the region of the analysis. If they were really there, we would expect to find about 70% of the single-particle strength concentrated in the observed fragments as illustrated in Fig. 8(c) rather than about 10% as actually observed and illustrated in Fig. 8(d). Even if this problem of interpretation were ignored, interference effects similar to those shown in Fig. 7 would make it nearly impossible to fit the observed widths of levels close to the $2p$ state. The reduction of r_b to 3.86 fm moves all but the quasistable $1d_{3/2}$ state upward (Fig. 6) and results in better agreement between the observed widths of the fragments and the locations of the single-particle states.

Finally, an inner radius is critical for subtraction of the $1d_{3/2}$ state. The "$d_{3/2}$-$1d_{3/2}$" curve in Figs. 2 or 3 would be quite negative (−25° at 6 MeV) if r_b were 7 fm. The curve for 3.86 fm leads to a good fit to the data; in fact, the fit above 3.4 MeV could be improved by reducing r_b to 3.5 fm in order to make the "$d_{3/2}$-$1d_{3/2}$" curve even more positive.

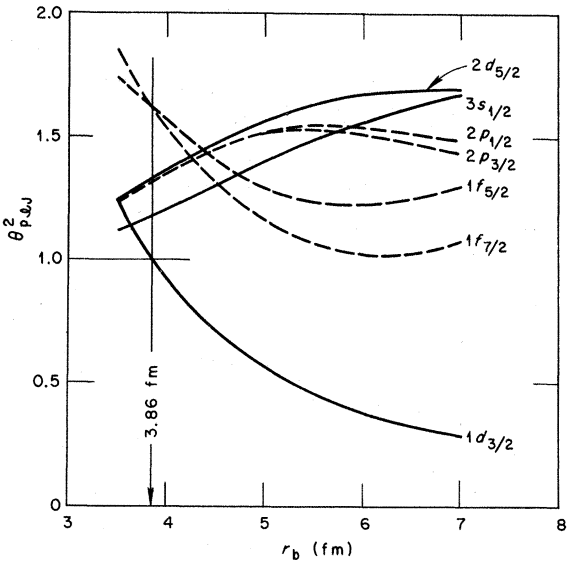

FIG. 9. Dimensionless single-particle reduced widths, $\theta^2 = \gamma^2/(\hbar^2/\mu r_b{}^2)$, for the first unbound states with natural boundary conditions for radii inside the potential tail. Solid and dashed curves refer to the even and odd potentials.

Figure 10 shows curves for R^{∞}_{lJ} calculated from Eq. (14) or (15) for $r_b = 3.86$ fm. These all increase almost linearly with energy. Those for $s_{1/2}$ and $d_{5/2}$ are negative because the nearby $2s_{1/2}$ and $1d_{5/2}$ states are bound, and those for p and f waves show the effects of the higher $2p$ and $1f$ levels. The "$d_{3/2}$-$1d_{3/2}$" curve is nearly constant because the $2d_{3/2}$ state is very far away.

The boundary parameters, b_{lJ}, are chosen to make S^0_{lJ} vanish at the energies shown by the arrows in Fig. 10. The $d_{3/2}$ condition is the natural one and is carefully chosen for Eq. (15). For the other partial waves b_{lJ} is not so important because the exact R functions rather than the expansions are used in the analysis. Actually, one could get into difficulties by choosing b_{lJ} so poorly that it places one of the single-particle levels too close to our energy region. The off-resonant phase shifts would then still be correct, but interference with the single-particle level could make it nearly impossible to fit a local level except with a very large reduced width. This phenomenon would occur, for example, if the s-wave boundary condition were chosen to make S^0 vanish near 2.3 MeV where the potential scattering is near 90° even though there is no true single-particle resonance. (In retrospect, this report might read better if natural boundary conditions had been used also for p and f waves, but the fact that the final reduced widths for the isolated levels are consistent with those from single-level analyses shows that no serious single-particle interference effects have been introduced by the boundary conditions.)

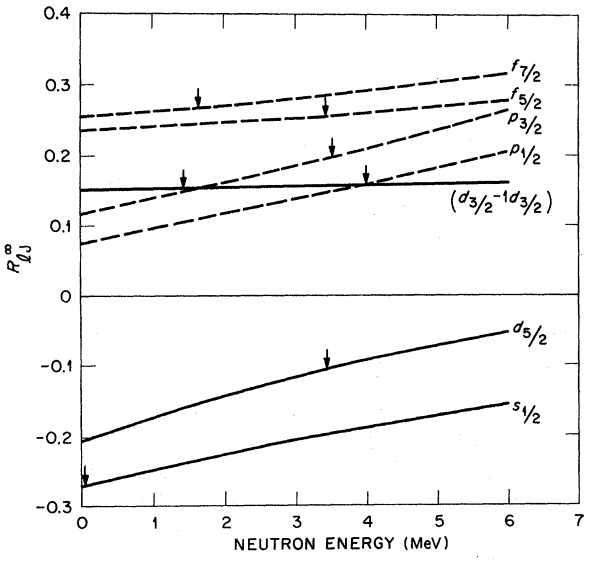

FIG. 10. Curves of R^{∞}_{lJ} from Eqs. (14) and (15) for a 3.86-fm radius and boundary conditions that make the shift functions vanish at the energies of the arrows. The solid and dashed curves refer to the even and odd potentials.

V. ALPHA-PARTICLE CHANNEL

For the $^{16}O(\alpha, n)^{13}C$ reaction the spins and parities are such that $l_\alpha = l_n \pm 1$ for $J = l_n \pm \frac{1}{2}$. To simplify the notation let us use only the subscript $l \equiv l_n$ with the understanding that the α-particle penetrabilities and shift factors are to be calculated correctly with $l_\alpha = l \pm 1$. The elastic scattering matrix element is given by[2]

$$U_{lJ}e^{-2i\varphi_{lJ}} = 1 + 2i\,P_{lJ}d^{-1}\{R^n_{lJ} - L^\alpha_{lJ}[R^n_{lJ}R^\alpha_{lJ} - (R^{n\alpha}_{lJ})^2]\}, \quad (18)$$

where

$$d = (1 - R^n_{lJ}L^n_{lJ})(1 - R^\alpha_{lJ}L^\alpha_{lJ}) - L^n_{lJ}(R^{n\alpha}_{lJ})^2L^\alpha_{lJ}$$

and L^n_{lJ} and L^α_{lJ} are the usual functions of shift and penetration factors. For the three R functions, R^n_{lJ} is the same as in Eq. (11) and, with the neglect of the α-particle widths outside of our energy region,

$$R^\alpha_{lJ} = \sum_{\lambda=1}^{N_{lJ}} \gamma_{\lambda\alpha lJ}{}^2/(E_{\lambda lJ} - E) \quad (19)$$

and

$$R^{n\alpha}_{lJ} = \sum_{\lambda=1}^{N_{lJ}} \gamma_{\lambda n lJ}\gamma_{\lambda\alpha lJ}/E_{\lambda lJ} - E). \quad (20)$$

For consistency I use a real diffuse-edge potential for the α channel and place the boundary inside the potential tail; the parameters are from Fig. 9 of the paper of Michaud, Scherk, and Vogt.[12]

By analogy with the single-channel approximation, I define the observed α-particle width as

$$\Gamma_{\lambda\alpha lJ} = 2P^\alpha_{lJ}\gamma_{\lambda\alpha lJ}{}^2, \quad (21)$$

where the penetrability P^α_{lJ} is calculated at the α-particle energy corresponding to the neutron resonant energy E_r. This width is about the same as from a single-level analysis if multilevel interference is negligible in the α channel. If $\Gamma_{\lambda n lJ} > \Gamma_{\lambda\alpha lJ}$, the definition of $\Gamma_{\lambda n lJ}$, as given in the text following Eq. (13), is nearly the same as the neutron width that would be obtained from a single-level analysis. It is *not* the total width.

VI. R-MATRIX FIT

The fits to the data were obtained visually. Figure 11 shows the total cross sections from 0.2 to 5.8 MeV. The points are measurements obtained with a $^7Li(p, n)$ source in the companion paper[3] and the crosses are from Wisconsin.[4-7] Narrow resonances not included in the R matrix are indicated by X or R. The lower figures are the partial cross sections. Table I lists the level parameters with

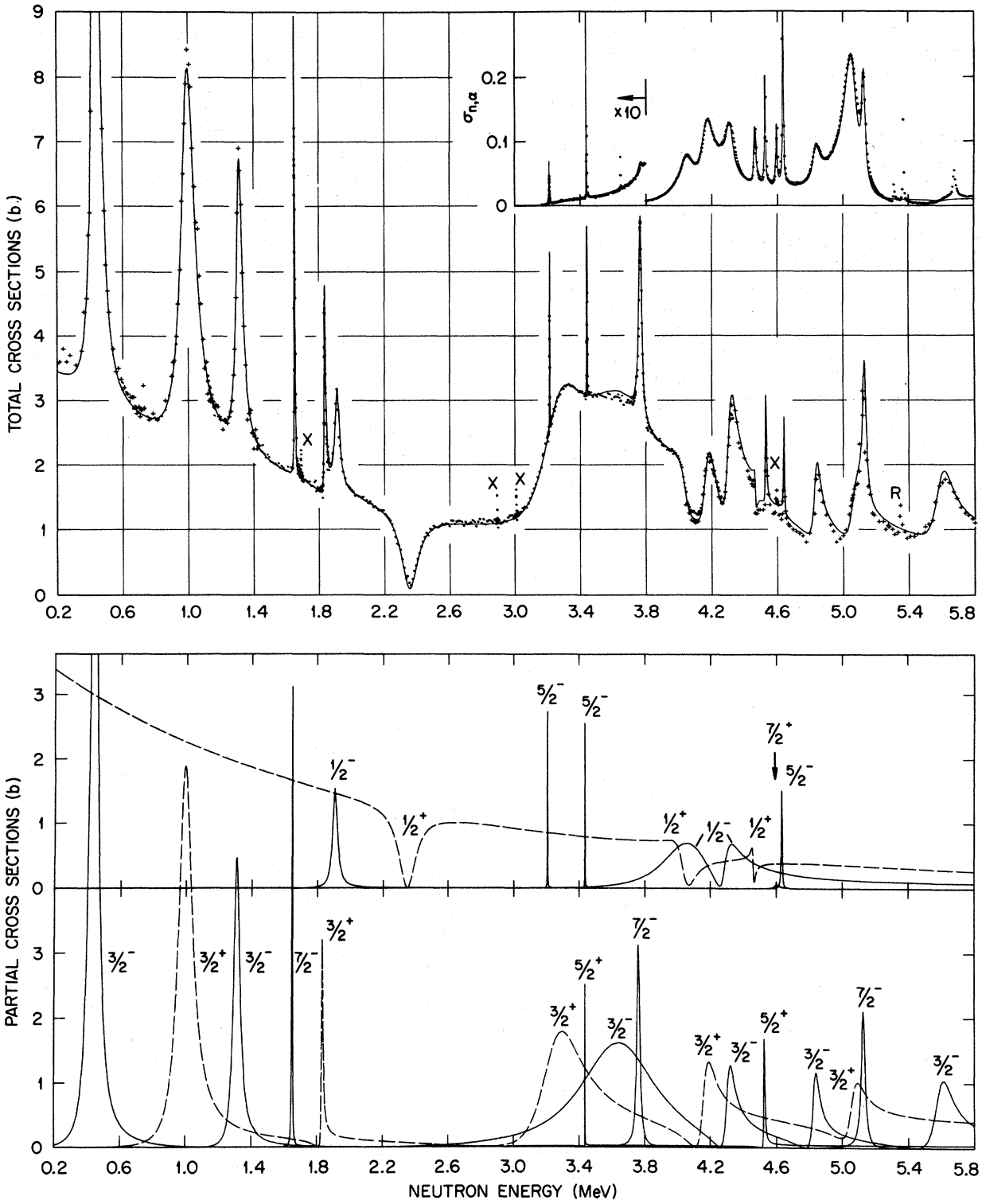

FIG. 11. The R-matrix fit to the total neutron cross sections of ^{16}O. In the main upper figure the dots are from the companion paper (Ref. 3) and the crosses from the University of Wisconsin (Refs. 4–7). Partial cross sections are in the lower figure. Part of Fig. 12 is inserted at the upper right.

level numbers referring to the first 41 known excited states[3] in ^{17}O. The primary experimental data for the assignments of widths and energies are indicated by footnotes in the table.

The angle-integrated (n, α) cross sections are shown in the insert at the upper right in Fig. 11 and also in Fig. 12, which includes the partial (n, α) cross sections. The data are deduced from measurements on the inverse reaction by Bair and Haas.[8] Since these workers used a flat response 4π detector, their excitation function has the right shape except for finite resolution effects. They quote a ±20% absolute uncertainty; I have reduced their absolute cross sections by 20% to give better agreement with the average from several investigations[8, 26, 27] and to make it easier to obtain a fit consistently with the total cross sections. The $\frac{3}{2}^+$ resonance at 3.3 MeV is included to fit the broad flat region in Fig. 12.

In regard to Table I, the definition of E_λ and E_r are given above. The energy E_{peak} refers to the point where the real phase shift is an odd multiple of $\pi/2$ and where the total cross section is a maximum. The energy E^{α}_{peak} corresponds to the (n, α) peak for the given partial wave. The excitation energy E_{ex} in ^{17}O is computed from E_r with $Q = 4142.6$ keV. Of these energies, only E_λ enters directly into the R matrix. In regard to the widths, $\gamma_{\lambda n}{}^2$ enters directly into the R matrix and the α-particle width $\Gamma_{\lambda\alpha}$ enters indirectly. The signs assumed for the products $\gamma_n \gamma_\alpha$ are listed in the last column. The other widths are derived quantities. The observed width $\Gamma_{\lambda n}$ is defined above following Eqs. (13) and (21).

The product $2P_n \gamma_{\lambda n}{}^2$ is included in the table for comparison to $\Gamma_{\lambda n}$. It is seen that $\Gamma_{\lambda n} \simeq 2P\gamma_{\lambda n}{}^2$ for the narrow isolated resonances; thus, a single-level analysis for each of these would lead to re-

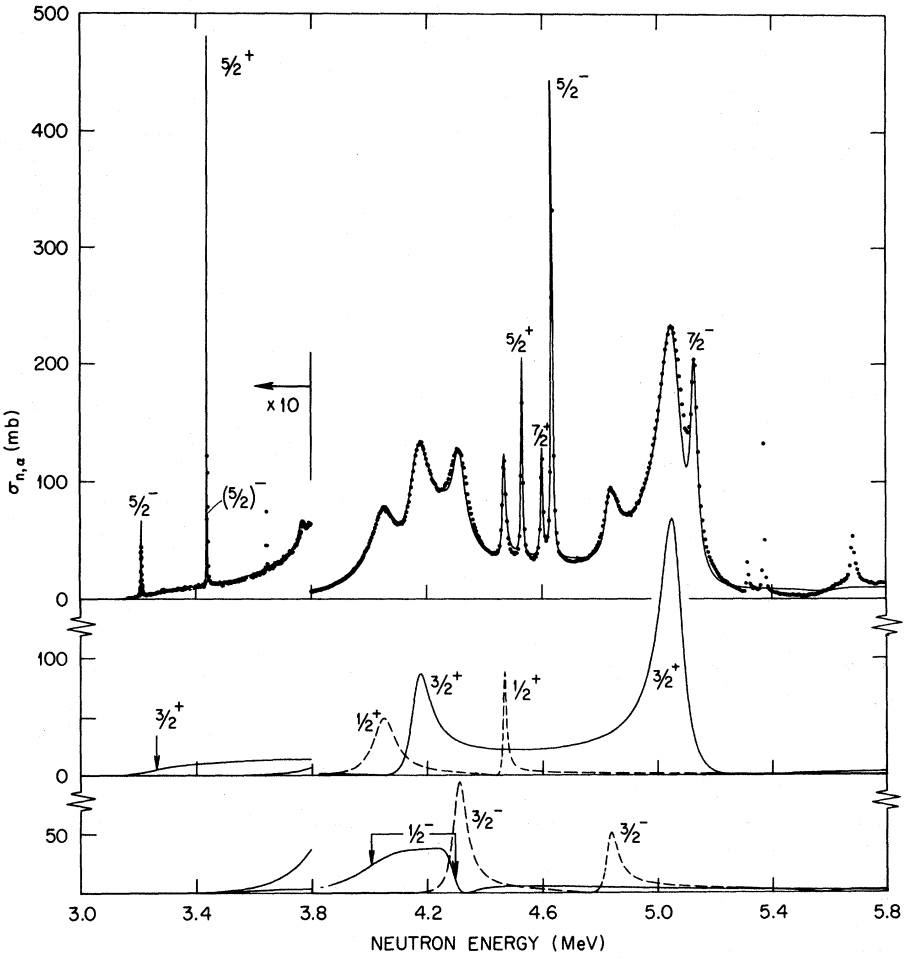

FIG. 12. Fit to the angle-integrated $^{16}O(n,\alpha)^{13}C$ cross sections. The points are from data on the inverse reactions by Bair and Haas (Ref. 8) normalized by a factor of 0.8. The lower figures show partial cross sections.

duced widths in essential agreement with the multilevel analysis. For isolated but broad resonances, such as the one at 442 keV, the product disagrees with the observed width because of the variations in penetrability, shift factor, and potential scattering over the width of the resonance. For the strongly overlapping levels, whether some of them are broad or not, the product disagrees strongly with the observed width. In these cases a single-level analysis would not be valid. This is so particularly for the five $\frac{3}{2}^+$ states.

VII. DISCUSSION

Most of the individual levels are discussed in the companion paper.[3] The $\frac{1}{2}^+$ and $\frac{1}{2}^-$ assignments are determined from the total cross sections. In regard to the $\frac{3}{2}^+$ and $\frac{3}{2}^-$ states it is interesting to speculate on how many of the parities could have been assigned from this broad-range fit without the aid of angular distributions. The presence of the broad $\frac{3}{2}^+$ 1-MeV resonance makes the other $\frac{3}{2}^+$ resonances much less symmetric than those for

TABLE I. Parameters of fit to σ_T and $\sigma_{n,\alpha}$.

		Energies [a] (lab)					Widths [a] (c.m.)					
J^π	^{17}O Level No. [b]	E_λ (keV)	E_{peak} (keV)	E^α_{peak} (keV)	E_r (keV)	E_{ex} (keV)	$\gamma_{\lambda n}{}^2$ (keV)	$\theta_{\lambda n}{}^2$ (%)	$2p_n\gamma_{\lambda n}{}^2$ (keV)	$\Gamma_{\lambda n}$ (keV)	$\Gamma_{\lambda\alpha}$ [c] (keV)	$\frac{\Gamma_{\lambda n}\Gamma_{\lambda\alpha}}{\lvert\Gamma_{\lambda n}\Gamma_{\lambda\alpha}\rvert}$
$\frac{1}{2}^+$	12 [d]	2367 [e]			2351	6354	24	0.81	115	124		
	23 [f]	4061 [g]		4051	4048	7950	14	0.47	80	84	6.7	+1
	28 [d]	4470 [g]		4470	4469	8347	1.8	0.06	10.5	10	2.2	+1
$\frac{1}{2}^-$	11 [d]	1906 [e]	1908		1908	5937	15	0.51	32	31.5		
	24 [h]	3980 [e]	4063		4090	7990	100	3.4	380	250	14	+1
	26 [h]	4305 [e]	4346		4289	8177	20	0.68	81	68	0.8	−1
$\frac{3}{2}^-$	4 [d]	399 [i]	443		442		129	4.4	55	45		
	7 [d]	1310 [i]	1313		1312	5377	27	0.91	42	41.5		
	19 [d]	3540 [e]	3649		3632	7559	150	5.1	560	500	0.08	+1
	27 [d]	4321 [g]	4323	4313	4310	8197	12.7	0.43	53	48	4.0	+1
	33 [d]	4830 [g]	4840	4840	4833	8689	10.5	0.36	47	42	1.8	+1
	41 [j]	5586 [i]	5630		5610	9420	27	0.91	130	120		
$\frac{3}{2}^+$	5 [d]	709 [i]	1000		1000	5083	2035	68.9	180	96		
	10 [d]	1838 [e]	1834		1833	5867	28	0.95	9.6	6.6		
	16 [d]	3536 [e]	3295		3248	7198	500	16.9	515	280	0.12	+1
	25 [d]	4311 [g]	4191	4179	4167	8062	252	8.5	394	71	15	+1
	34 [d]	5156 [g]	5085	5051	5054	8897	123	4.2	260	68	9.7	−1
$\frac{5}{2}^+$	17	3438 [e]	3438	3438	3438	7377	0.35	0.01	0.2	0.5	0.01	+1
	29	4537 [g]	4532	4532	4532	8406	2.3	0.08	5.1	4.8	0.54	+1
$\frac{5}{2}^-$	15	3208 [e]	3211		3211	7163	14	0.47	1.4	1.4	0.0027	+1
	18	3441 [e]	3441	3441	3441	7380	9.7	0.33	1.2	1.2	0.0032	+1
	32	4644 [g]	4637	4637	4637	8505	11.8	0.40	3.5	3.4	1.9	+1
$\frac{7}{2}^-$	8	1651 [e]	1651		1651	5696	277	9.4	3.6	3.4		
	21 [k]	3815 [e]	3766	3766	3766	7685	95	2.9	15.4	18	0.01	+1
	36	5188 [g]	5131	5131	5131	8969	45	1.5	20	23	2.3	+1
$\frac{7}{2}^+$	30 [l]	4601 [g]	4601	4601	4601	8471	1.6	0.53	0.03		7.6	+1

[a] Subscripts $l\,J$ are implied by J^π.

[b] Level number refers to Table III of Ref. 3. Bound levels No. 1, $\frac{5}{2}^+$ and No. 2, $\frac{1}{2}^+$ included effectively in R^∞ for real well. Bound levels Nos. 3 and 4 and narrow unbound levels Nos. 6, 9, 13, 14, 20, 22, 31, 35, 37–40, and 42 are omitted from analysis.

[c] All $\Gamma_{\lambda\alpha}$ to fit (n, α) cross sections of Ref. 8 normalized (×0.8).

[d] Spin and parity from Ref. 20 confirmed.

[e] Energies assigned from measurements of σ_T in companion paper (Ref. 3).

[f] Parity of level established by analysis.

[g] Energies chosen to fit (α, n) data from Ref. 8.

[h] Level discovered and J^π assigned.

[i] Energies assigned from Wisconsin data on σ_T from Refs. 4–7.

[j] J^π assigned by present analysis of Wisconsin data from Ref. 6.

[k] J value confirmed.

[l] Analysis shows that this level not No. 31 observed in σ_T in Ref. 6.

$\frac{3}{2}^-$, and it seems probable that most of these parities could have been assigned if the 1-MeV resonance were the only one known initially. In any case there is little chance that any of the $\frac{1}{2}^-$, $\frac{1}{2}^+$, $\frac{3}{2}^+$, or $\frac{3}{2}^-$ resonances have the wrong assignment.

The cluster of (n, α) resonances from 3.4 to 5.2 in Fig. 12 shows interesting interference between the two $\frac{3}{2}^+$ resonances. This occurs because of the $\gamma_n\gamma_\alpha$ term in Eq. (20). If the sign of this product is the same for the two levels, the cross section vanishes at some energy between resonances, but if the sign is different, it does not. The large contribution between resonances, which is predicted by opposite signs, accounts for the observed background. The J^π values of these two resonances was deduced previously from $^{13}C(\alpha, n)$ and $^{13}C(\alpha, \alpha)$ angular distributions.[28] It is important[3] to verify these particular assignments and this fit to the interference pattern is a verification. The peak for the $\frac{1}{2}^-$ doublet (24 and 26) also has an unusual shape; the sign of $\gamma_n\gamma_\alpha$ must be different for the two members.

Probably the most interesting results are embodied in the neutron dimensionless reduced widths, $\theta_{\lambda n}{}^2$. In Fig. 13 the known levels with $J \leq \frac{7}{2}$ and $l \leq 3$ below 9.5 MeV in ^{17}O are represented by symbols with areas proportional to the dimensionless reduced widths. The bound and first excited states are shown as ~100% on the basis of (d, p) stripping.[21] The other two bound states have spectroscopic factors[20] of about 3%. A few unbound levels with very small widths are shown as dots and the symbols for the remaining levels represent the dimensionless widths from Table I. The sums for these unbound states are shown at the top of the figure.

The $d_{3/2}$ sum is significant. The unit sum means that the total widths for the five observed states is nearly equal to the width of the $1d_{3/2}$ single-particle state. This justifies the subtraction of the entire $1d_{3/2}$ state from the potential R function. The centroid of eigenenergies for the five states is 5.74 MeV, whereas the eigenenergy for the potential is 5.47 MeV; this discrepancy would be removed by trivial adjustments in the well parameters. (The centroid is defined by $\sum_\lambda \gamma_\lambda{}^2 E_\lambda / \sum_\lambda \gamma_\lambda{}^2$ for the five levels.)

The small sums for $\frac{5}{2}^+$ and $\frac{1}{2}^+$ show that below 9.5 MeV in ^{17}O there are negligible $s_{1/2}$ and $d_{5/2}$ fragments other than the ground and first excited states, and they justify our use of an R function which concentrates all of the $2s_{1/2}$ and $1d_{5/2}$ strengths in those two states. The (d, p) stripping analysis[21] had already given spectroscopic factors of 1.0 ± 0.2 for those states, and the fact that there is negligible additional strength up to 9.5 MeV suggests that the spectroscopic factors are at least 90%.

An interpretation of the p and f fragments must be more qualitative because the dimensionless widths, particularly for f waves, may differ by 30 to 50% from the spectroscopic factors. Since there are no bound f states the observed f-wave resonances are associated with the unbound $1f$ levels. The strengths in Fig. 13 are consistent with the levels in Fig. 6 for the 3.86-fm radius. The p-wave fragments could arise from either the bound $1p$ or unbound $2p$ states. Since the spin-orbit effect enhances the contribution from the un-

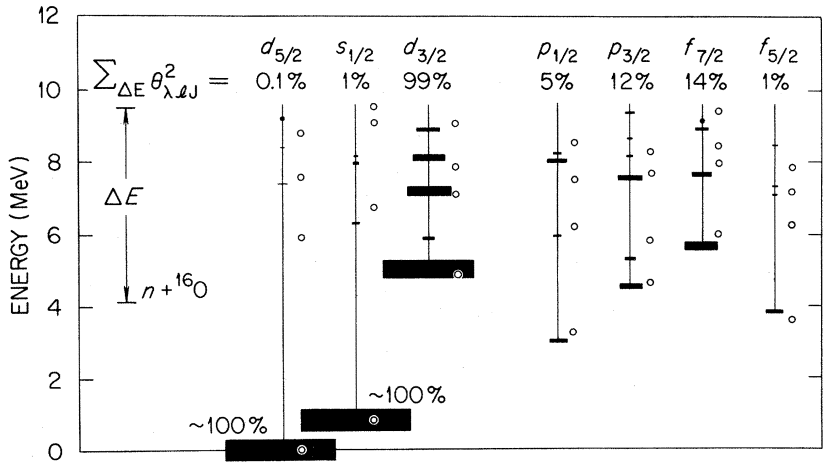

FIG. 13. Observed fragmentation of single-particle strengths below 9.5 MeV in ^{17}O. The areas of the symbols represent approximate spectroscopic factors. The unbound states and the sums are from Table I. Shell-model energy calculations (Ref. 29) for the first four levels of each partial wave are shown by small circles to the right of each scheme. Some of the known levels (Ref. 3) at 5.21, 5.73, 6.86, 6.97, 7.57, and 8.48 might belong in this figure.

bound $2p_{3/2}$ state, the relatively large reduced widths for the observed $\frac{3}{2}^-$ states suggest that these come mostly from the $2p_{3/2}$ orbit. For the $\frac{1}{2}^-$ states, shell-model calculations[29] indicate that the bound and at least some of the unbound states have strengths imported from the $1p_{1/2}$ orbital. A comparison with the 3.86-fm structure in Fig. 6 shows qualitative agreement. Certainly the observed fragments are not consistent with the 7-fm structure.

In Fig. 13 the small circles show the energies for the first four levels of each partial wave from shell-model calculations by Wildenthal and McGrory.[29] These authors treat five particles in the $1p_{1/2}$, $1d_{5/2}$, and $2s_{1/2}$ orbits around an inert ^{12}C core. Even though the $1d_{3/2}$ orbit is not included, the predicted levels show fairly good one-to-one correspondence with those observed. Of course, neutron spectroscopic factors are not predicated for other than the $1p_{1/2}$, $2s_{1/2}$, and $1d_{5/2}$ orbits. (Six more observed states[3] with unknown J^π may belong, in part, in this figure.)

In summary the total neutron and angle-integrated (n, α) cross sections for ^{16}O are well described by the multilevel analysis in which the distant bound and unbound levels are the single-particle states in a composite model which has a potential well for the bound and quasibound region and an R-matrix boundary radius chosen carefully inside the potential tail to give, with appropriate boundary conditions, the unbound states of the continuum. The potential is a Woods-Saxon well with a Thomas-type spin-orbit term and, since it is local,[30] its well depths are parity-dependent.

ACKNOWLEDGMENT

I am particularly grateful to Dr. Mark Reeves, III, for writing the code for calculating neutron wave functions, to Richard Feezel and Dwight Smith for helping in fitting the data, and to Dr. R. L. Becker and Dr. J. L. Fowler for many helpful discussions. Discussions with Dr. H. J. Kim, Dr. J. B. McGrory, Dr. P. A. Moldauer, Dr. J. R. Risser, Dr. G. R. Satchler, and Dr. E. P. Wigner are also gratefully acknowledged. I also appreciate the use of the data of Dr. J. K. Bair and Dr. F. X. Haas prior to publication.

---

*Research sponsored by the U. S. Atomic Energy Commission under contract with Union Carbide Corporation.

[1]E. P. Wigner and L. Eisenbud, Phys. Rev. 72, 29 (1947).

[2]A. M. Lane and R. G. Thomas, Rev. Mod. Phys. 30, 257 (1958).

[3]J. L. Fowler, C. H. Johnson, and R. M. Feezel, to be published.

[4]A. Okazaki, Phys. Rev. 99, 55 (1955).

[5]H. R. Striebel, S. E. Darden, and W. Haeberli, Nucl. Phys. 6, 188 (1958).

[6]D. B. Fossan, R. L. Walter, W. E. Wilson, and H. H. Barschall, Phys. Rev. 123, 209 (1961).

[7]J. C. Davis and F. T. Noda, Nucl. Phys. A134, 361 (1969).

[8]J. K. Bair and F. X. Haas, Phys. Rev. C (to be published).

[9]D. Vautherin and M. Vénéroni, Phys. Letters 26B, 552 (1968).

[10]A. D. MacKellar, J. F. Reading, and A. K. Kerman, Phys. Rev. C 3, 460 (1971).

[11]C. B. Dover and N. V. Giai, Nucl. Phys. A177, 559 (1971).

[12]E. Vogt, Rev. Mod. Phys. 34, 723 (1962); E. Vogt, G. Michaud, and H. Reeves, Phys. Letters 19, 570 (1965); G. Michaud, L. Scherk, and E. Vogt, Phys. Rev. C 1, 864 (1970).

[13]G. D. Westin and J. L. Adams, Phys. Rev. C 4, 363 (1971).

[14]J. L. Fowler and H. O. Cohn, Phys. Rev. 109, 89 (1958).

[15]J. P. Schiffer, Nucl. Phys. 46, 246 (1963).

[16]T. Teichman and E. P. Wigner, Phys. Rev. 87, 123 (1952).

[17]K. Takeuchi and P. A. Moldauer, Phys. Rev. C 2, 920, 925 (1970).

[18]B. Buck, Neutron Bound State Calculations (unpublished).

[19]M. Reeves, III, Code PSDDBG (unpublished).

[20]F. Ajzenberg-Selove, Nucl. Phys. A166, 1 (1971).

[21]I. M. Naqib and L. L. Green, Nucl. Phys. A112, 76 (1968).

[22]*Neutron Cross Section*, compiled by J. R. Stehn, M. D. Goldberg, B. A. Magurno, and R. Wiener-Chasman, Brookhaven National Laboratory Report No. BNL-325 (U.S. GPO, Washington, D. C., 1966), 2nd ed., 2nd Suppl.

[23]C. H. Johnson and J. L. Fowler, Phys. Rev. 162, 890 (1967).

[24]D. Lister and A. Sayres, Phys. Rev. 143, 745 (1966).

[25]J. L. Fowler and C. H. Johnson, Phys. Rev. C 2, 124 (1970).

[26]R. B. Walton, J. D. Clement, and F. Boreli, Phys. Rev. 107, 1065 (1957).

[27]K. K. Sekharan, A. S. Divatia, M. K. Mehta, S. S. Kerekatte, and K. B. Nambiar, Phys. Rev. 156, 1187 (1967).

[28]B. K. Barnes, T. A. Belote, and J. R. Risser, Phys. Rev. 140, B616 (1965).

[29]B. H. Wildenthal and J. B. McGrory, private communication also quoted by M.-C. Lemaire, M. C. Mermaz, and K. K. Seth, Phys. Rev. C 5, 328 (1972).

[30]An expanded version of this paper is available from the author and contains comments on an energy-dependent, parity-independent potential as well as more detailed discussions of other aspects.